minerals

MDPI

Article

Effect of Ball Filling Ratio on Fine Particle Production Characteristics During Ceramic Ball Grinding of Magnetite Ore

Li Ling [1,2], Chengfang Yuan [3,4,*], Liying Sun [4], Caibin Wu [1,2,*], Quan Li [2], Ziyu Zhou [2] and Zongyan Zhou [3,4]

[1] School of Resources and Environmental Engineering, Jiangxi University of Science and Technology, Ganzhou 341000, China
[2] Jiangxi Provincial Key Laboratory of Low-Carbon Processing and Utilization of Strategic Metal Mineral Resources, School of Resources and Environmental Engineering, Jiangxi University of Science and Technology, Ganzhou 341000, China
[3] Jiangxi Provincial Key Laboratory of Particle Technology, Jiangxi University of Science and Technology, Nanchang 330013, China
[4] Research Centre for Intelligent Mineral Processing & Metallurgy, International Institute for Innovation, Jiangxi University of Science and Technology, Nanchang 330013, China
* Correspondence: chf.yuan@jxust.edu.cn (C.Y.); caibin.wu@jxust.edu.cn (C.W.); Tel.: +86-15779000805 (C.Y.); +86-13970145667 (C.W.)

Abstract

To clarify the influence of the media filling ratio on fine particle production during ceramic ball grinding of magnetite, magnetite ore from the fine grinding stage of an industrial concentrator was investigated under different feed size classes and media filling ratios through grinding kinetics experiments. The generation behavior of the fine and finest particle fractions during ceramic ball grinding was systematically analyzed. The results indicate that particle size fractions with sizes less than or equal to 0.150 mm exhibit pronounced zero-order production characteristics under different filling ratios, with cumulative yields showing a strong linear relationship with grinding time. This zero-order behavior is insensitive to variations in the media filling ratio. Conversely, the generation rate of the finest size fraction is significantly affected by the media filling ratio. For coarse feed sizes, the generation rate of the finest fraction initially increases and then decreases with increasing filling ratio, reaching a peak value of 6.23%/min at a filling ratio of 35%. When the feed falls below 1.18 mm, the generation rate of the finest fraction shows a strong positive correlation with the ceramic ball filling ratio. Furthermore, based on the functional relationship between the generation rate of the finest size fraction and the mill input power, an energy–size model for magnetite ceramic ball grinding was established, providing a quantitative description of the variation in the finest particle yield with respect to the input energy and media filling ratio. The findings provide a theoretical foundation for optimizing media filling ratios, enhancing fine grinding performance, and controlling overgrinding in industrial applications.

Keywords: ceramic ball grinding; magnetite ore; zero-order production characteristics; ball mill

Check for updates

Academic Editor: Carlos Hoffmann Sampaio

Received: 23 January 2026
Revised: 15 February 2026
Accepted: 25 February 2026
Published: 28 February 2026

Copyright: © 2026 by the authors. Licensee MDPI, Basel, Switzerland. This article is an open access article distributed under the terms and conditions of the Creative Commons Attribution (CC BY) license.

1. Introduction

The media in a ball mill is defined as the volume of grinding media in a static state relative to the effective volume of the mill, and it is a key operational parameter that governs the internal motion of the media, collision behavior, and energy transfer characteristics during the grinding process [1,2]. Variations in the filling ratio can significantly alter

the frequency of media–media and media–particle collisions, as well as the energy per collision, thereby influencing the comminution mechanism and the particle size distribution of the milled product [3,4]. Since the introduction of ball milling, the media filling ratio has been a central focus in both grinding research and industrial practice. In the 1960s, Bond [5] conducted a systematic investigation of the media filling ratio in the context of the Bond work index theory. Subsequently, Kelsall [6] reported that the filling ratio can significantly affect grinding performance by modulating the first-order linear breakage kinetics of ores. Later studies have predominantly examined the topic indirectly through rotation speed [7,8], grinding kinetic modeling [9,10], or numerical simulation of media motion [11–14], while systematic studies directly addressing the effect of media filling ratio on fine particle generation remain limited, particularly in non-steel ball grinding systems [15].

In mineral processing, fine grinding is typically employed to achieve sufficient liberation of valuable minerals [16–18]. However, the generation of fine particles during grinding can significantly affect subsequent separation processes [19–23]. Due to their high specific surface area and surface activity, fine mineral particles are susceptible to non-selective adsorption and mechanical entrainment during flotation and other separation operations, with their generation characteristics and quantity closely linked to separation performance [22–25]. Previous studies have shown that moderate particle size reduction can enhance recovery, whereas excessive fining may diminish separation efficiency, suggesting that the overproduction of fine particles can adversely affect downstream processes. Nevertheless, the mechanisms governing fine particle generation during grinding and the factors influencing their formation remain poorly understood [26]. As a key parameter affecting grinding intensity and media–particle interactions, the media filling ratio has not been systematically investigated with respect to its influence on fine particle generation.

Ceramic ball grinding refers to a process in which low-density ceramic balls partially or fully replace conventional steel balls as the grinding media. In comparison to conventional steel ball grinding, the use of ceramic ball grinding modifies the media density, elastic modulus, and energy transfer characteristics, leading to varied ore breakage modes and patterns of fine particle generation [27–29]. In recent years, the application of ceramic ball grinding has been increasingly applied in the fine grinding stages of mineral processing plants in China [30–34]. The increasing demand for processing complex and low-grade ore bodies has imposed higher requirements on grinding product quality [35]. For these micro-fine and refractory iron ores, the grinding product's particle size distribution plays a decisive role in the efficiency of downstream separation. Recent investigations have demonstrated that the recovery performance of flotation intensification equipment and combined magnetic–gravity separation circuits is highly sensitive to feed particle size characteristics [36,37]. These findings underscore the importance of controlling fine particle generation during grinding. Therefore, precise control of the grinding fineness via ceramic media has become a critical operational requirement. However, the majority of existing studies have concentrated on energy consumption and media size distribution [29,38,39], while the influence of the media filling ratio on fine particle generation and particle size outcomes under ceramic ball grinding conditions remains poorly understood.

Based on this, the present study utilizes magnetite from an industrial fine grinding circuit as the research material to systematically investigate the influence of the media filling ratio on fine particle generation characteristics during ceramic ball grinding, providing experimental evidence for understanding the behavior of fine particle formation under conditions of ceramic ball grinding conditions.

2. Materials and Methods

2.1. Characteristics of the Raw Ore

The experimental samples were collected from a typical magnetite beneficiation plant in Anhui Province, China. The feed material was obtained from the secondary ball mill following primary magnetic separation (the concentrate). The raw ore was classified using a set of standard sieves with aperture sizes of 2.360 mm, 1.180 mm, 0.600 mm, and 0.300 mm, resulting in three size fractions of magnetite ore: a coarse fraction (−2.360 + 1.180 mm), an intermediate fraction (−1.180 + 0.600 mm), and a fine fraction (−0.600 + 0.300 mm).

Each size fraction was thoroughly homogenized, after which representative subsamples were obtained by splitting for chemical composition and mineralogical analyses. The remaining material was prepared, packaged, and reserved for subsequent grinding experiments. The multi-element chemical compositions of the three size fractions are presented in Table 1, and the mineralogical characteristics determined by X-ray diffraction (XRD) are illustrated in Figure 1.

Table 1. Chemical multi-element classification results of experimental samples.

Sample	Element Content/%						
	Fe	Si	Ca	S	Al	Mg	K
Coarse particles	47.45	17.15	14.38	6.61	5.08	2.94	1.91
Medium particles	48.25	16.72	14.60	6.59	5.06	2.92	1.74
Fine particles	53.07	14.53	13.23	6.39	4.39	2.87	1.47

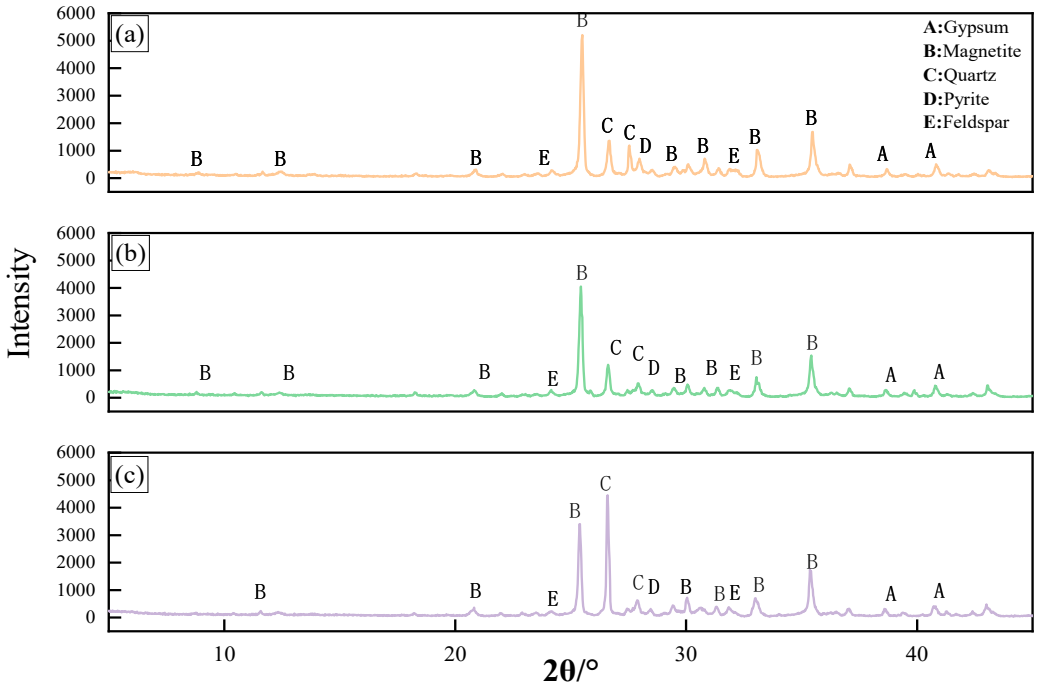


Figure 1. XRD analysis results of the test sample.

As presented in Table 1, following the initial magnetic separation, the Fe grade of the samples was significantly enhanced compared with that of typical magnetite ores, with an average value nearing 50%. In oxidized magnetite ores, silicate gangue minerals generally exhibit relatively high hardness and are more resistant to breakage. As a result, silicate minerals tend to remain in coarser size fractions in the grinding products, leading

to a comparatively lower Fe grade in the coarse magnetite fraction. This occurrence is frequently observed in magnetite beneficiation plants.

X-ray diffraction (XRD) analysis indicates that the dominant diffraction peaks of all size fractions correspond to magnetite, confirming that magnetite is the predominant mineral phase, accompanied by minor amounts of pyrite. Owing to the acidic and high-hardness characteristics of the magnetite ore in this deposit, a certain proportion of silicate minerals, such as quartz, is also present in the phase assemblage. The major mineral phases and their respective contents for the three size fractions are summarized in Table 2.

Table 2. Major mineral phases and their contents in the test samples.

Magnetite Ore	Mineral Content/%						
	Quartz	K-Feldspar	Magnetite	Calcite	Gypsum	Pyrite	Clay Minerals
Coarse particles	18.40	4.70	64.33	2.00	5.50	2.80	1.30
Medium particles	8.91	2.13	66.72	3.52	8.68	5.23	2.32
Fine particles	7.21	1.23	71.67	3.90	9.40	3.05	3.35

As shown in Table 2, the three size fractions exhibit similar major mineralogical compositions, with magnetite contents exceeding 64% in all samples, indicating that they are representative magnetite ores. With decreasing particle size, the magnetite content shows an increasing trend, and the fine fraction contains the highest magnetite proportion, reaching 71.67%. In contrast, the coarse fraction is characterized by a relatively high quartz content of 18.40%, which is more than twice that of the intermediate and fine fractions. Overall, the experimental samples contain relatively high proportions of gangue minerals, including quartz and gypsum.

To characterize the mechanical properties of the raw ore, several representative irregular magnetite lumps with particle sizes of approximately 8 mm, 10 mm, 15 mm, 20 mm, 25 mm, and 30 mm were selected from the crushing section of the beneficiation plant and subjected to uniaxial compressive strength tests. The results of the pressure test results conducted of the irregular ore lumps are summarized in Table 3.

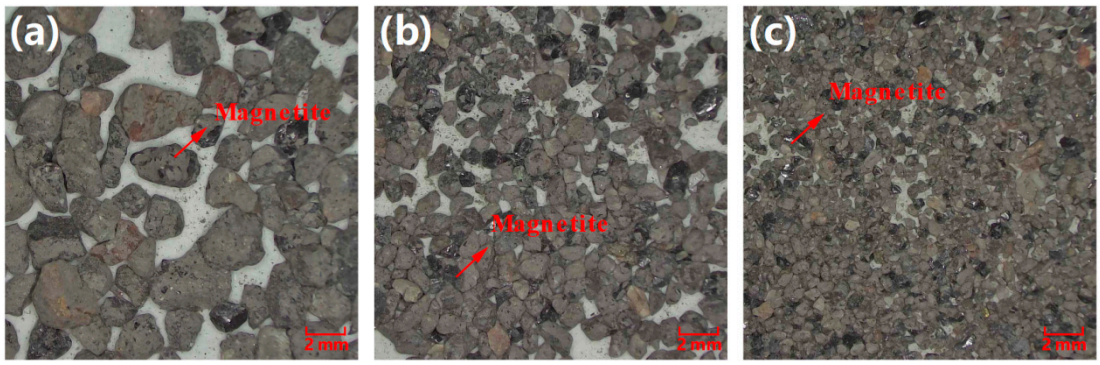
Table 3. Pressure test results of irregular ore blocks.

Size (mm)	Compressive Strength (kg/cm^2)	Compressive Strength (Mpa)	Protodyakonov Hardness (f)
8	494.41	49.44	4.94
10	531.77	53.18	5.32
15	955.17	95.52	9.55
20	854.95	85.50	8.55
25	602.58	60.02	6.02
30	544.00	54.40	5.44

As shown in Table 3, the uniaxial compressive strength of the irregular magnetite ore lumps is generally around 500 kg/cm^2 or higher, corresponding to a Protodyakonov strength coefficient (f) in the range of approximately 5–10, indicating that the ore can be classified as a relatively hard material. The variation in compressive strength with particle size does not follow a linear trend, and the magnetite ore lumps with particle sizes ranging from 15 to 20 mm demonstrate relatively higher compressive strength values.

Due to limitations associated with the compressive strength testing apparatus and sample preparation, we could not accurately measure the compressive strength of particles smaller than 8 mm. Nevertheless, according to the particle size effect and Griffith's crack propagation theory, when the particle size decreases below a critical threshold (typically around 3 mm), the number of pre-existing surface flaws is significantly reduced, resulting in a pronounced increase in the nominal compressive strength. Figure 2 presents the surface

morphologies of magnetite ores across three different size fractions, as observed under an optical microscope.



(a)Coarse particle-size magnetite; (b)Medium particle-size magnetite; (c)Fine particle-size magnetite

Figure 2. Surface morphology of test samples.

The experimental samples were sourced from an industrial magnetite ore processing circuit. As shown in Figure 2, the surfaces of most magnetite particles are coated with a layer of fine clay minerals, resulting in relatively indistinct surface morphological features, particularly for the coarse size fraction. With decreasing particle size, repeated screening operations induce mechanical scrubbing effects, leading to partial exposure of the black magnetite minerals and a clearer definition of particle surface contours.

2.2. Experimental Methods

The grinding media filling ratio is a critical operating parameter in mineral processing plants, as it directly affects energy consumption and mill throughput. An increase in the media filling ratio typically improves grinding performance and allows for a moderate increase in mill capacity; however, it is also accompanied by higher power consumption and grinding media wear. To systematically investigate the influence of media filling ratio on the grinding kinetics of magnetite ore under ceramic ball grinding conditions, a series of batch grinding kinetic experiments were performed at various media filling ratios.

In this study, an XMQ 240 × 90 laboratory ball mill was used as the grinding device. Three size fractions of magnetite ore were utilized as the grinding feed, comprising a coarse fraction with particle sizes of −2.360 + 1.180 mm, an intermediate fraction of −1.180 + 0.600 mm, and a fine fraction of −0.600 + 0.300 mm. Grinding tests were carried out for grinding times of 1, 2, 3, 4, and 5 min under ceramic ball filling ratios of 20%, 25%, 30%, 35%, and 40%. The pulp density was maintained at 70%, and the mill speed was consistently set at 90% of the critical speed throughout all experiments.

After grinding, each product sample was subjected to particle size analysis using a series of standard sieves. Particles in the size range of −0.600 to +0.038 mm were classified by wet sieving, whereas particles finer than 0.038 mm were separated using a hydraulic sedimentation method. During wet sieving, the standard sieves were immersed in a water-filled container, and the ground material was sieved under water. The water was replaced every 1 to 2 min until it remained clear, indicating the completion of the wet sieving process. Subsequently, the retained and passing products of each size fraction were dried and weighed to determine the particle size distribution and corresponding yield. The overall experimental procedure is illustrated in Figure 3. The sieve aperture sizes utilized in this study were 0.425 mm, 0.300 mm, 0.212 mm, 0.150 mm, 0.106 mm, 0.075 mm, 0.053 mm, 0.045 mm, and 0.038 mm.

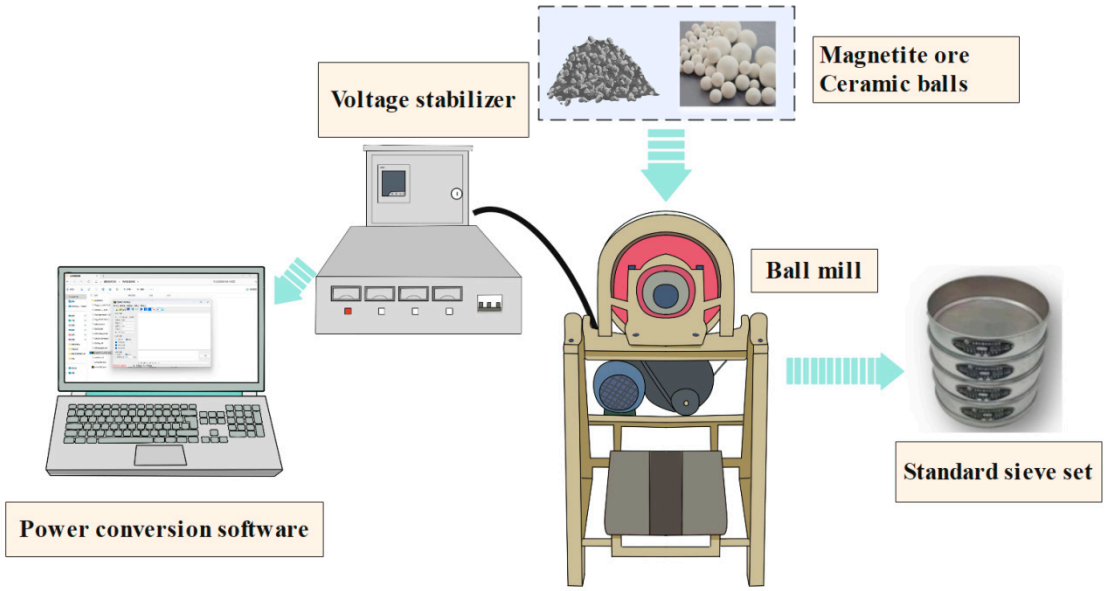


Figure 3. Schematic diagram of the filling ratio test for ceramic ball grinding.

2.3. Zero-Order Production Characteristics

Zero-order production characteristics delineate the grinding behavior of fine particles during short grinding durations, where the breakage ratio of a single size fraction or the coarsest size fraction does not exceed 65%. Under these conditions, the formation of finer size fractions in the grinding products can be approximated by zero-order kinetics, in which the cumulative undersize yield increases linearly with grinding time [40]. This relationship can be expressed as follows:

$$\frac{dP(d,t)}{dt} = F(d) \tag{1}$$

where $P(d,t)$ represents the cumulative undersize yield of particles smaller than size d at grinding time t, and $F(d)$ denotes the zero-order cumulative production rate constant corresponding to particle size d.

The value of $F(d)$ varies with particle size and is typically characterized by the following empirical relationship:

$$F(d_i) = kd_i^{\alpha} \tag{2}$$

where k and α are fitting constants. The parameter α primarily reflects the intrinsic breakage characteristics of the material and is generally weakly dependent on the operating state of the ball mill. However, when significant changes in breakage mode occur, such as when steel balls are replaced with ceramic balls as the grinding media, the value of α may also be influenced.

Zero-order production characteristics are primarily employed to quantify the generation rate of fine particles during grinding and are particularly valuable for analyzing overgrinding behavior. A smaller α value indicates that the fine particle production rate varies more slowly with particle size, resulting in more similar production characteristics among different fine size fractions and a more uniform particle size distribution.

2.4. Discrete Element Method

The DEM is an effective approach for studying particle systems, offering distinct advantages in the analysis of particle behavior [41,42]. The DEM was introduced by Cundall and Strack [43] in the 1970s and has since been extensively utilized in particle research in past decades. For this study, the commercial DEM software of Rocky® (version: 25R1) was employed. According to Newton's second law of motion, individual particles

can experience both translational and rotational motions. The equations governing the translational and rotational motions of a particle, characterized by its mass and moment of inertia, can be expressed as follows:

$$m_i \frac{d\mathbf{v}_i}{dt} = \sum_{j=1}^{k_c} \left(\mathbf{f}_{c,ij} + \mathbf{f}_{d,ij} \right) + m_i \mathbf{g} \tag{3}$$

$$I_i \frac{d\boldsymbol{\omega}_i}{dt} = \sum_{j=1}^{k_c} \left(\mathbf{M}_{t,ij} + \mathbf{M}_{r,ij} \right) \tag{4}$$

where $\mathbf{v}_i$ and $\boldsymbol{\omega}_i$ represent the velocity and rotational speed of particle i, respectively, and k_c represents the number of particles in contact with particle i, including the wall action. The forces involved are gravity $m_i\mathbf{g}$ and inter-particle forces, including elastic contact forces $\mathbf{f}_{c,ij}$ and viscous damping forces $\mathbf{f}_{d,ij}$. These inter-particle forces can be decomposed into normal and tangential lines. The moments acting on i by particle j include $\mathbf{M}_{t,ij}$ from tangential forces, and $\mathbf{M}_{r,ij}$ from rolling friction.

The contact parameters related to the ball mill and stirred mill used in the numerical simulation are listed in Table 4.

Table 4. Particle properties and DEM parameters used in the simulation.

Parameter	Value
Particle shape	spherical
Particle diameter (mm)	30 (media)
Particle density (kg/m^3)	3750 (ceramic ball)
Coefficient of static friction	0.3 (ball–ball), 0.7 (ball–liner)
Coefficient of sliding friction	0.15 (ball–ball), 0.15 (ball–liner)
Coefficient of restitution	0.353 (ball–ball) 0.50 (ball–liner)
Poisson's ratio	0.3
Young's modulus	1×10^7
Time step (s)	10×10^{-6}

3. Experimental Results

3.1. PSD of Grinding Products for Coarse Magnetite Ore

The curves obtained by plotting the yield of each size fraction as a function of particle size are referred to as partial particle size distribution curves. These curves provide a direct representation of the size fraction distribution of grinding products and their variation under different operating conditions. For the coarse magnetite ore fraction with a feed size of −2.360 + 1.180 mm, the partial particle size distribution curves of the grinding products obtained at various ceramic ball filling ratios and grinding durations are displayed in Figure 4.

As grinding time increased, the grinding products of coarse magnetite ore under different ceramic ball filling ratios exhibited a consistent trend of first decreasing the size fraction yield and then increasing the finest fraction yield. When the ceramic ball filling ratio was below 30%, the partial particle size distribution curves displayed a bimodal pattern, with peak size fractions at +1.18 mm and −0.038 mm. The first size fraction +1.18 mm exhibited a breakage ratio not exceeding 70%, and the finest fraction −0.038 mm accounted for a significantly higher proportion compared with other size fractions. At a filling ratio of 25% and a grinding time of 5 min, the yield of the −0.038 mm fraction peaked at 32.44%.

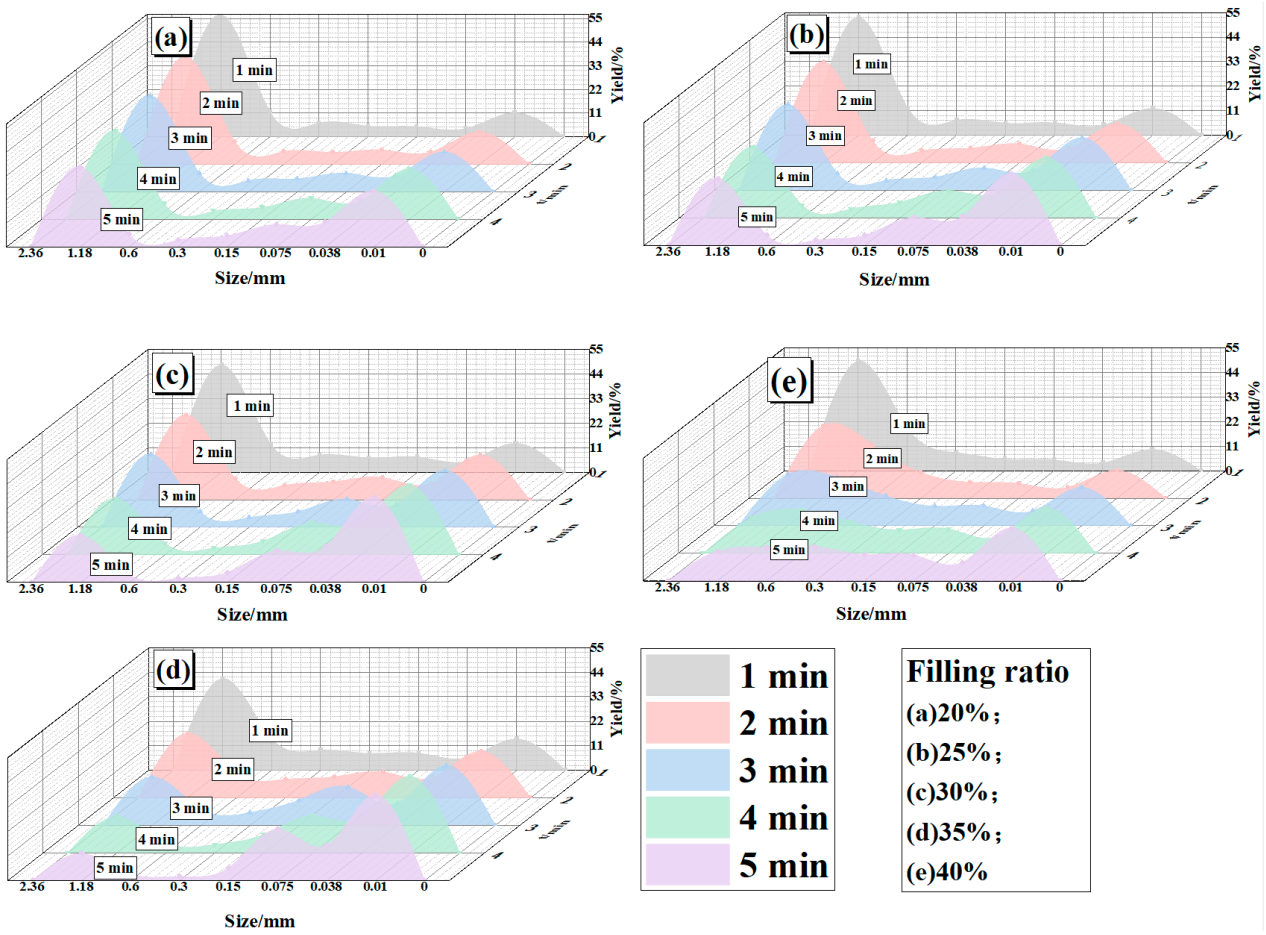


Figure 4. PSD for coarse magnetite ore under different ceramic ball filling ratios.

When the ceramic ball filling ratio was between 30% and 40%, the partial particle size distribution curves transitioned from a bimodal to a trimodal pattern, with an additional peak at −0.15 + 0.075 mm. In this range, the breakage ratio of the first size fraction increased significantly to nearly 90%, and the grinding products exhibited a more even distribution compared to those obtained at lower filling ratios.

At a filling ratio of 40%, the partial particle size distribution curves reverted to a bimodal pattern. Compared with low filling ratios, the curves exhibited lower and smoother peaks, and the transfer of material from the first size fraction to the finest fraction was diminished. Notably, at a grinding time of 5 min, the yields of all size fractions except the finest fraction were nearly uniform.

3.2. PSD of Grinding Products for Intermediate Magnetite Ore

Figure 5 presents the partial particle size distribution curves of intermediate magnetite ore with a feed size of −1.180 + 0.600 mm under different ceramic ball filling ratios. These curves offer a direct illustration of the variation in size fraction yields of the grinding products.

The partial particle size distribution curves of intermediate magnetite ore with a feed size of −1.180 + 0.600 mm displayed significant differences compared to those of the coarse fraction, consistently exhibiting a trimodal pattern across ceramic ball filling ratios from 20% to 40%. At a filling ratio of 20%, the breakage ratio of the first size fraction +0.6 mm reached 85.19%, increasing to 94.35% when the filling ratio was 30%. Under conditions of a low filling ratio, the peaks of the trimodal distribution corresponded to +0.6 mm, −0.15 +0.075 mm, and −0.038 mm. The first size fraction was more evenly distributed

compared with the coarse fraction, indicating that a reduction in feed size significantly enhances the breakage capacity of the mill under low filling ratio conditions, thereby resulting in improved grinding performance.

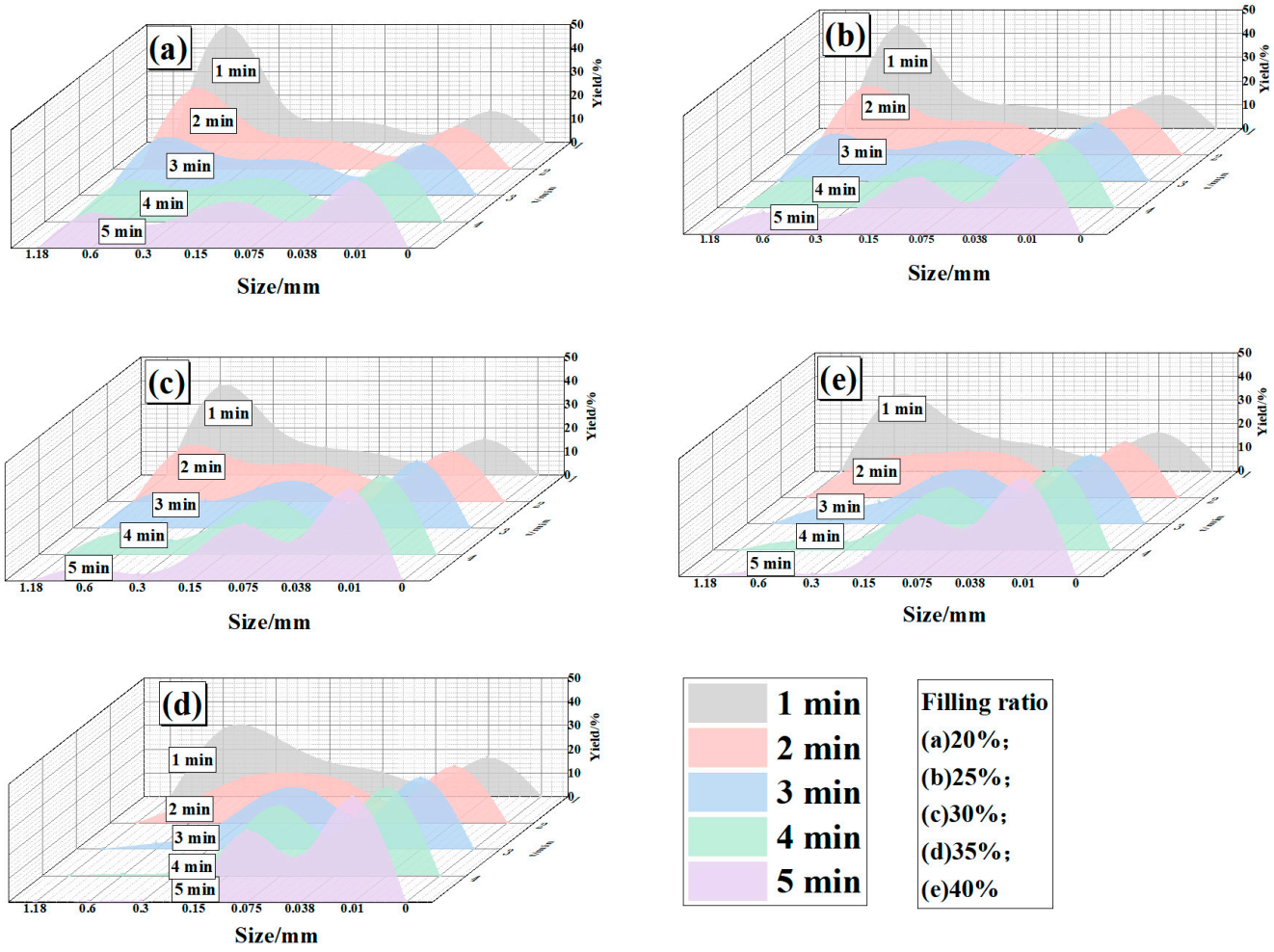


Figure 5. PSD for intermediate magnetite ore under different ceramic ball filling ratio.

At a filling ratio of 35%, the breakage ratio of the first size fraction approached 100%, and its characteristic peak gradually disappeared with increasing grinding time. When the grinding time exceeded 3 min, the partial particle size distribution curves transitioned from a trimodal to a bimodal pattern, indicating that the grinding process progressed from primary to secondary breakage.

At a filling ratio of 40%, the curves fully exhibited a bimodal pattern. In comparison with lower filling ratios, the curves shifted to the right and the average particle size of the products decreased significantly. When the grinding time exceeded 3 min, the breakage ratio of the second size fraction surpassed 90%, corresponding to multiple repeated breakage within the mill. Simultaneously, the proportion of the finest fraction increased sharply, reaching 44.44% for the −0.038 mm fraction at 5 min.

3.3. PSD of Grinding Products for Fine Magnetite Ore

Figure 6 shows the partial particle size distribution curves of fine magnetite ore with a feed size of −0.600 + 0.300 mm under different ceramic ball filling ratios.

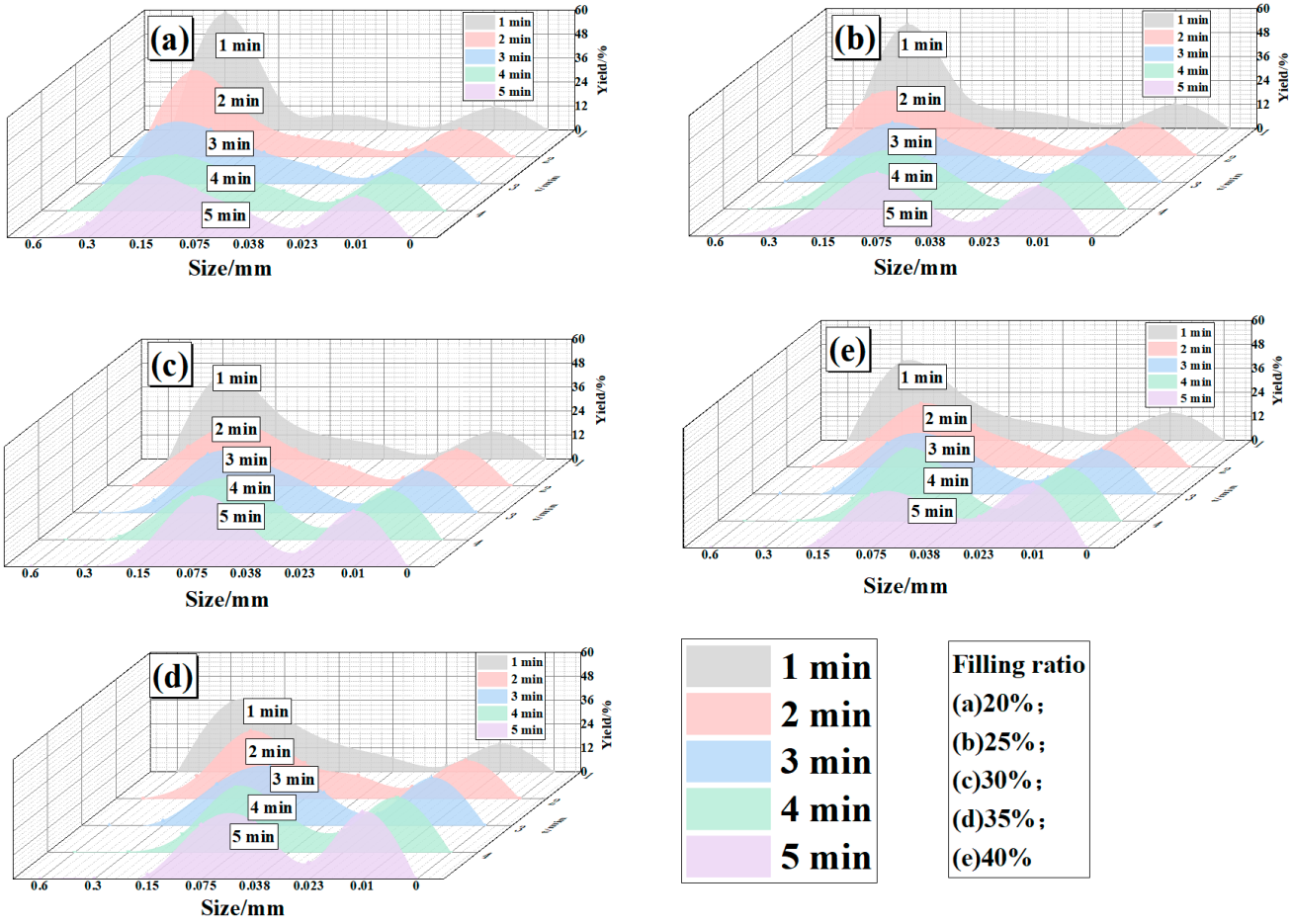


Figure 6. PSD for fine magnetite ore under different ceramic ball filling ratio.

As the feed size was progressively decreased, the partial particle size distribution curves of fine magnetite ore under ceramic ball grinding conditions reverted from the trimodal pattern observed for the intermediate fraction to a bimodal distribution resembling that of the coarse fraction.

At a ceramic ball filling ratio of 20%, the breakage ratio of the first size fraction +0.3 mm reached 92.87%, which was 30.26 percentage points higher than that of the coarse fraction subjected to ceramic ball grinding. As the filling ratio increased to 30%, the breakage ratio of the first size fraction approached 100%, and the primary peak of the partial particle size distribution curves gradually shifted from the first size fraction +0.3 mm to the second size fraction −0.3 + 0.075 mm, indicating that secondary breakage became dominant within the mill. When the filling ratio was further increased to above 35%, the breakage ratio of the second size fraction also approached 100%, and the grinding process became increasingly characterized by multiple cycles of repeated breakage.

Given the relatively fine feed size of the magnetite ore, the use of −0.038 mm as the finest size fraction was insufficient to fully characterize the particle size distribution. Therefore, −0.019 mm was introduced as the finest size fraction for fine magnetite ore grinding. At a filling ratio of 30%, the yield of the −0.019 mm fraction was 28.02%, while it increased to 33.92% at a filling ratio of 40%. Although the increase in the filling ratio significantly enhanced the breakage of the first size fraction, the proportion of the finest fraction did not increase substantially. This indicates that ceramic ball grinding of fine magnetite ore at higher filling ratios effectively suppresses excessive generation of ultrafine particles, resulting in a more uniform particle size distribution.

4. Analysis and Discussion

4.1. Fine Particle Production Characteristics

Variations in the ceramic ball filling ratio directly affect the breakage rate function and the cumulative particle size distribution during grinding, thus affecting the generation behavior of fine particles. Based on the zero-order production characteristics, the fine particle generation rates during the ceramic ball grinding of coarse magnetite ore under different filling ratios were analyzed. The fine particle production rate functions at different ceramic ball filling ratios are shown in Figure 7, and the corresponding kinetic parameters were obtained by linear regression and are summarized in Table 5.

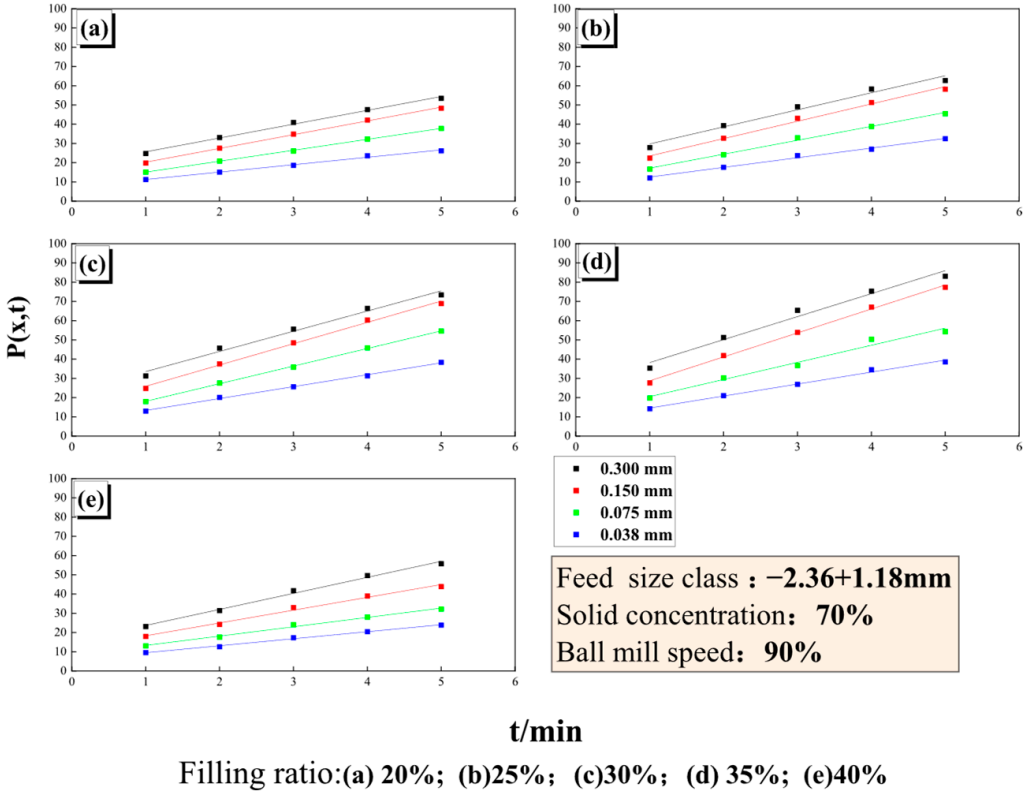


Figure 7. Fine generation rate in the ceramic ball grinding product of coarse magnetite ore.

Using coarse magnetite ore as the grinding feed, the negative cumulative undersize yields of the four finest sub-size fractions (0.300 mm, 0.150 mm, 0.075 mm, and 0.038 mm) were considered as dependent variables, while grinding time was used as the independent variable for linear regression analysis. The slope of the fitted straight line was defined as the fine particle generation rate for each size fraction.

For the 0.300 mm size fraction, the average adjusted R^2 value was approximately 0.98, which did not exceed 0.99, indicating a relatively weak linear relationship between the cumulative undersize yield and grinding time. In contrast, when the particle size was smaller than 0.150 mm, a strong linear relationship was observed, with adjusted R^2 values generally exceeding 0.99. These results indicate that, for size fractions smaller than or equal to 0.150 mm, the generation rate is predominantly independent of grinding time, demonstrating pronounced zero-order production characteristics. Therefore, in the grinding of coarse magnetite ore, sub-size fractions with particle sizes $\leq$ 0.150 mm can be classified as typical zero-order production fractions.

Table 5. Parameters of the fine particle generation rate function (coarse particle feed).

Feed Size Class		Coarse			
Filling Ratio	**Size**	**0.300 mm**	**0.150 mm**	**0.075 mm**	**0.038 mm**
20%	Intercept	18.453	13.112	9.389	7.410
	Slope	7.188	7.149	5.684	3.846
	R^2	0.995	0.999	1.000	0.994
	adj.R^2	0.994	0.998	0.999	0.992
25%	Intercept	20.871	14.485	9.927	7.513
	Slope	8.870	9.014	7.233	5.020
	R^2	0.979	0.992	0.996	0.992
	adj.R^2	0.972	0.990	0.994	0.990
30%	Intercept	23.006	14.800	8.901	7.143
	Slope	10.498	11.076	9.156	6.188
	R^2	0.986	0.996	0.999	0.998
	adj.R^2	0.981	0.995	0.999	0.997
35%	Intercept	26.240	16.253	11.604	8.366
	Slope	11.953	12.454	8.900	6.226
	R^2	0.979	0.997	0.979	0.993
	adj.R^2	0.972	0.996	0.972	0.991
40%	Intercept	15.356	11.650	8.430	5.851
	Slope	8.336	6.661	4.855	3.645
	R^2	0.993	0.991	0.993	0.995
	adj.R^2	0.991	0.988	0.990	0.994

At low ceramic ball filling ratios, the specific breakage rate of the initial size fraction was relatively low, resulting in limited breakage of the coarse particles within the same grinding time and, consequently, a relatively low generation rate of the finest fraction (−0.038 mm). As the ceramic ball filling ratio increased, the generation rate of the finest fraction gradually increased, reaching a maximum value of 6.226%·min^{-1} at a filling ratio of 35%. However, with a further increase in the filling ratio to 40%, the generation rate of the finest fraction decreased markedly to 3.645%·min^{-1}, corresponding to a reduction of 41.46%.

The fine particle generation rate functions for the ceramic ball grinding of intermediate magnetite ore under different filling ratios are presented in Figure 8. The corresponding kinetic parameters were obtained by linear regression and are summarized in Table 6.

Using intermediate magnetite ore as the grinding feed, the negative cumulative undersize yields of the four finest sub-size fractions (0.300 mm, 0.150 mm, 0.075 mm, and 0.038 mm) were also taken as dependent variables for linear regression analysis with grinding time. For the 0.300 mm size fraction, the average adjusted R^2 value was only 0.93, with a minimum value of 0.848, indicating no significant linear relationship between the cumulative undersize yield and grinding time and, therefore, the absence of zero-order production characteristics.

In contrast, when the particle size was smaller than 0.150 mm, a strong linear relationship between the cumulative undersize yield and grinding time was observed, with adjusted R^2 values generally exceeding 0.99. This indicates that the generation rate of these fine size fractions is independent of grinding time, demonstrating pronounced zero-order production characteristics. These results suggest that, similar to coarse magnetite ore grinding, sub-size fractions with particle sizes $\leq$ 0.150 mm in the intermediate grinding of magnetite ore can be considered typical zero-order production fractions.

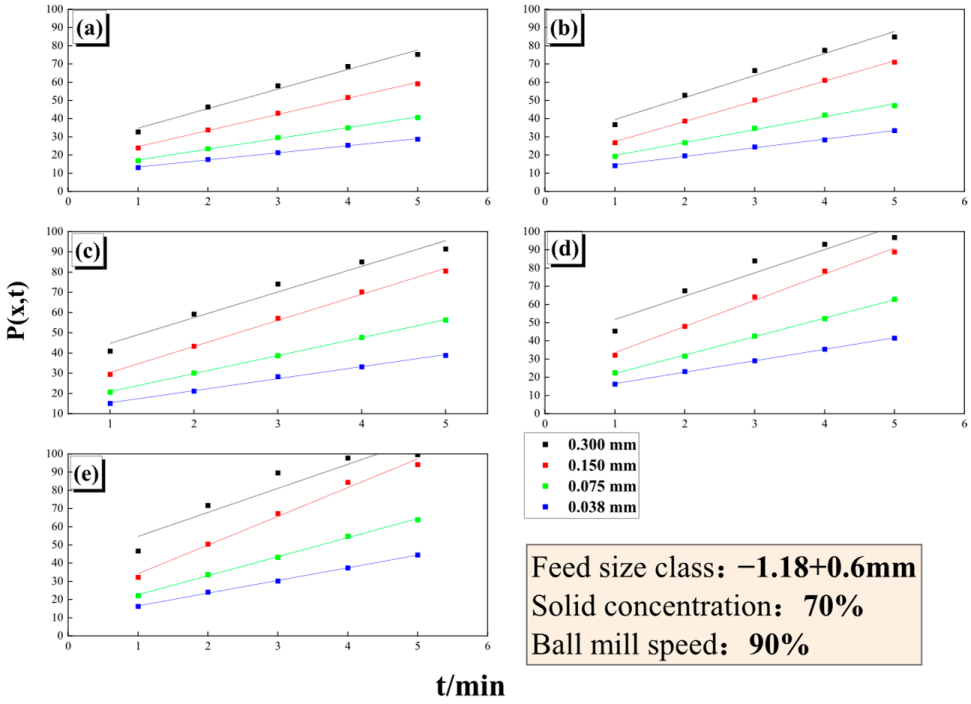


Figure 8. Fine generation ratio in the ceramic ball grinding product of intermediate magnetite ore.

Table 6. Parameters of the fine particle generation rate function (intermediate particle feed).

Feed Size Class		Intermediate			
Filling Ratio	**Size**	**0.300 mm**	**0.150 mm**	**0.075 mm**	**0.038 mm**
20%	Intercept	24.000	15.749	11.408	9.519
	Slope	10.736	8.845	5.898	3.889
	R^2	0.985	0.997	0.998	0.998
	adj.R^2	0.980	0.996	0.998	0.997
25%	Intercept	27.357	16.269	12.672	9.770
	Slope	12.105	11.089	7.089	4.730
	R^2	0.981	0.999	0.994	0.997
	adj.R^2	0.974	0.998	0.993	0.996
30%	Intercept	32.106	17.477	12.043	9.443
	Slope	12.689	12.883	8.890	5.955
	R^2	0.967	0.997	1.000	0.997
	adj.R^2	0.956	0.996	1.000	0.996
35%	Intercept	38.877	19.130	11.938	10.206
	Slope	12.822	14.381	10.136	6.289
	R^2	0.922	0.994	0.999	0.999
	adj.R^2	0.896	0.992	0.999	0.999
40%	Intercept	41.442	18.359	12.144	9.551
	Slope	13.208	15.778	10.464	6.972
	R^2	0.886	0.990	0.998	0.999
	adj.R^2	0.848	0.987	0.998	0.999

As the ceramic ball filling ratio increased, the generation rate of the finest fraction rose steadily from 3.889%·min^{-1} to 6.972%·min^{-1}, without exhibiting a distinct maximum. This suggests that, within the range of filling ratios investigated, the generation of fine particles from the fine particle generation process of intermediate magnetite ore was not significantly suppressed by overgrinding effects.

The fine particle generation rate functions for ceramic ball grinding of fine magnetite ore under different filling ratios are shown in Figure 9, and the corresponding kinetic parameters obtained by linear regression are summarized in Table 7.

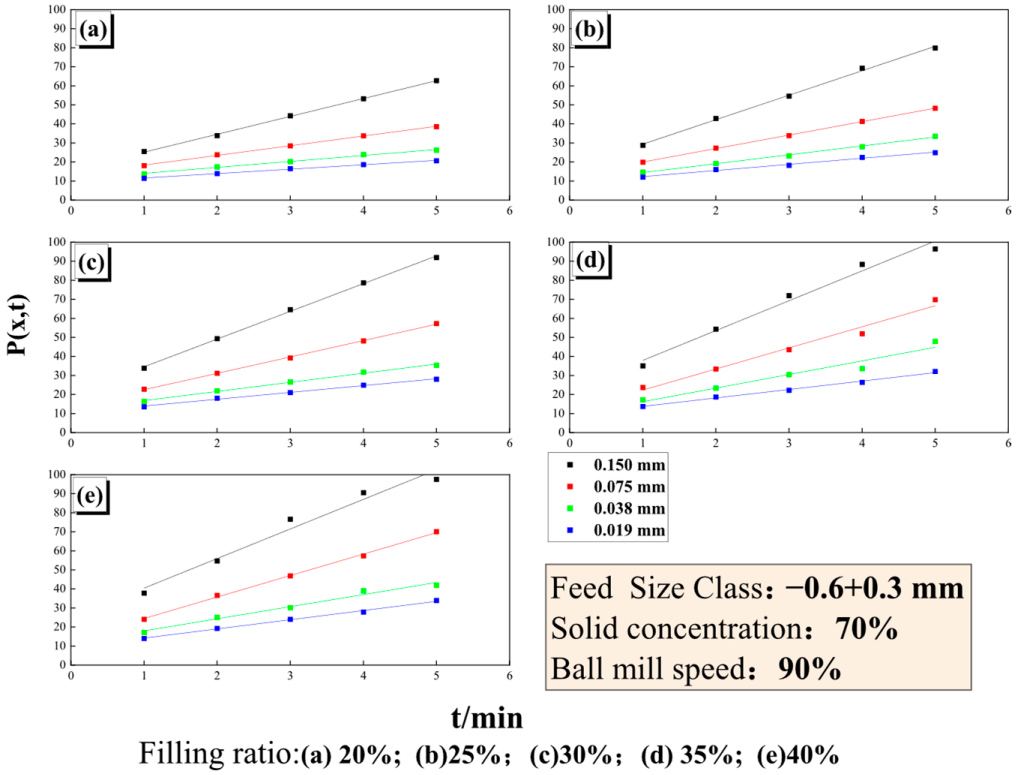


Figure 9. Fine generation rate in the ceramic ball grinding product of fine magnetite ore.

Table 7. Parameters of the fine particle generation rate function (fine particle feed).

Feed Size Class		Fine			
Filling Ratio	**Size**	**0.150 mm**	**0.075 mm**	**0.038 mm**	**0.019 mm**
20%	Intercept	15.771	13.246	10.882	9.260
	Slope	9.388	5.100	3.135	2.320
	R^2	0.999	0.999	0.994	0.997
	adj.R^2	0.999	0.999	0.993	0.996
25%	Intercept	16.492	12.901	9.764	9.095
	Slope	12.858	7.072	4.665	3.216
	R^2	0.998	1.000	0.996	0.992
	adj.R^2	0.997	0.999	0.995	0.990
30%	Intercept	19.969	13.897	12.003	10.347
	Slope	14.569	8.604	4.797	3.583
	R^2	0.999	0.999	0.995	0.996
	adj.R^2	0.999	0.999	0.993	0.994
35%	Intercept	22.223	11.233	9.069	9.326
	Slope	15.675	11.082	7.145	4.431
	R^2	0.982	0.979	0.949	0.994
	adj.R^2	0.976	0.972	0.932	0.991
40%	Intercept	24.866	13.201	11.604	9.343
	Slope	15.543	11.274	6.359	4.829
	R^2	0.971	0.998	0.982	0.996
	adj.R^2	0.962	0.998	0.976	0.994

Using fine magnetite ore as the grinding feed, the negative cumulative undersize yields of the four finest sub-size fractions (0.150 mm, 0.075 mm, 0.038 mm, and 0.019 mm) were utilized as dependent variables for linear regression analysis with grinding time. Owing to the pronounced occurrence of repeated breakage during the ceramic ball grinding of fine magnetite ore, the specific breakage rate increased with grinding time and further increased with a rising ceramic ball filling ratio.

For the −0.150 mm size fraction, the adjusted R^2 values of the linear fitting between cumulative undersize yield and grinding time gradually decreased with increasing filling ratio. When the filling ratio was lower than 30%, the adjusted R^2 values were consistently higher than 0.99, indicating pronounced zero-order production characteristics. However, when the filling ratio exceeded 30%, the intensified repeated breakage caused the adjusted R^2 to decrease sharply to 0.962, indicating that the zero-order production assumption was no longer valid for this size fraction. Therefore, variations in the ceramic ball filling ratio significantly affect the production characteristics of the −0.150 mm fraction, and repeated breakage at filling ratios above 30% leads to the loss of pronounced zero-order behavior.

For size fractions smaller than 0.150 mm, a strong linear relationship between cumulative undersize yield and grinding time was consistently observed, with adjusted R^2 values generally exceeding 0.99. These fractions demonstrate stable zero-order production characteristics that remain unaffected by variations in filling ratio or the occurrence of repeated breakage. With increasing ceramic ball filling ratio, the generation rate of the finest fraction increased from 2.320%·min^{-1} to 4.829%·min^{-1}, without exhibiting a distinct maximum.

4.2. Finest Size Fraction Generation Rate

For subsequent beneficiation processes, the generation rate of the finest size fraction directly determines the degree of slime formation in the grinding product. A higher degree of slime formation leads to an increased content of ultrafine particles, which not only deteriorates pulp rheological properties but also significantly impairs separation efficiency. Therefore, the generation rate of the finest size fraction serves as a crucial indicator for evaluating the rationality of grinding conditions and controlling overgrinding behavior.

In this study, the generation rate of the finest sub-size fraction was selected as the research focus to analyze the effect of the ceramic ball filling ratio on fine particle generation behavior. Specifically, for coarse and intermediate magnetite ore feeds, the −0.038 mm fraction was defined as the finest sub-size fraction, whereas for fine magnetite ore feed, the −0.019 mm fraction was designated as the finest size fraction. The variation in the generation rate of the finest size fraction under different filling ratios is illustrated in Figure 10.

Based on the aforementioned analyses, a highly significant linear relationship was observed between the cumulative undersize yield of the finest sub-size fraction and grinding time, with linear regression correlation coefficients exceeding 0.99 in all instances. Furthermore, this relationship exhibited insensitivity to variations in feed particle size and ceramic ball filling ratio. These findings indicate that, during the ceramic ball grinding of magnetite ore, the finest size fraction exhibits stable and pronounced zero-order production behavior, with its generation rate remaining essentially independent of grinding time within the explored range, indicating that the formation of ultrafine particles is weakly controlled by time.

As illustrated in Figure 10, the generation rate of the finest size fraction increases monotonically with increasing ceramic ball filling ratio. This phenomenon can be attributed to the fact that an increase in filling ratio does not significantly enhance the energy of individual collisions but substantially increases the number of grinding media within the mill, thereby raising the contact probability and effective collision frequency between

media and ore particles. Under such conditions, ore particles are more likely to undergo repeated low-energy, high-frequency breakage events dominated by abrasion, attrition, and compressive interactions, which promote the continuous generation of fine particles. The corresponding states of media motion and particle contact characteristics are schematically depicted in Figure 11.

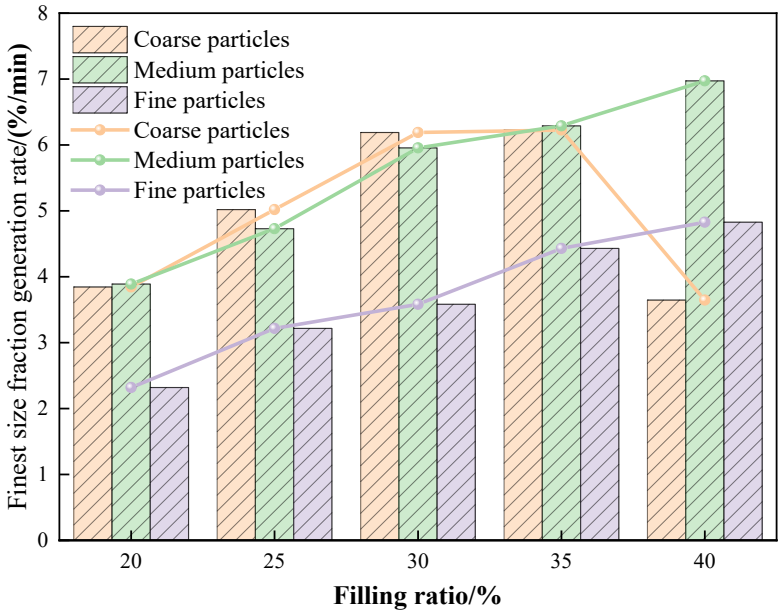


Figure 10. Effect of ceramic ball filling ratio on the generation rate of the −0.038 mm size fraction.

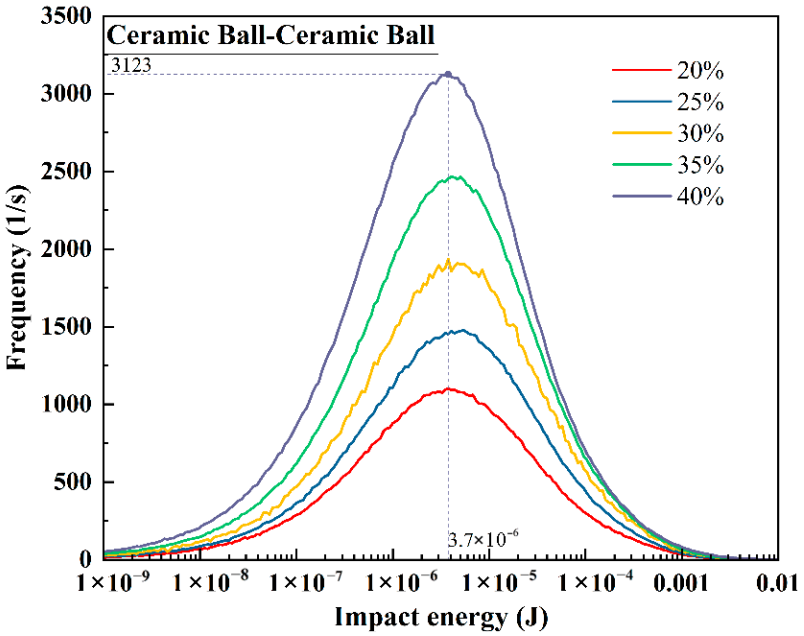


Figure 11. Collision energy spectrum of grinding media during ceramic ball grinding.

For coarse magnetite ore, the impact force generated by the cataracting motion of the grinding media serves as the primary breakage mechanism. As the ceramic ball filling ratio increases, the area of the cataracting zone expands, resulting in a higher specific breakage rate of the first size fraction and a corresponding increase in the generation rate of the finest fraction. However, when the filling ratio exceeds 35%, the proportion of the cataracting zone begins to decrease and its overall center of mass shifts downward, reducing the maximum impact force and causing a rapid decline in the finest fraction generation rate

(Figure 12). Therefore, for coarse magnetite ore, optimizing the filling ratio allows the minimization of overgrinding without compromising the desired fineness.

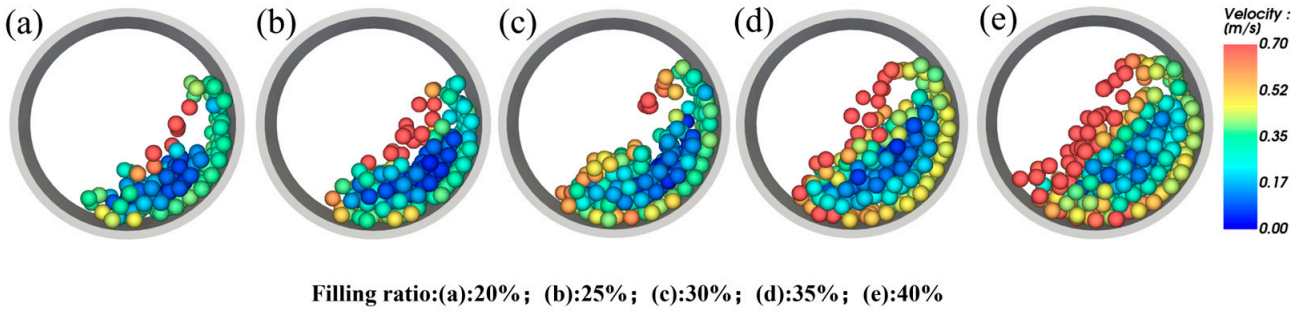


Figure 12. Collision cloud maps of grinding media during ceramic ball grinding under different filling ratios.

For intermediate and fine magnetite ore, the grinding force generated in the centrifuging (cascading) motion zone dominates the breakage process. With increasing filling ratio, the area of the centrifuging zone progressively enlarges, accelerating the generation rate of the finest size fraction. Consequently, increasing the filling ratio can significantly enhance overgrinding for intermediate magnetite ore (−1.180 mm) during ceramic ball grinding.

The different responses of coarse and fine particles to the filling ratio are fundamentally rooted in their distinct breakage mechanisms. Mechanically, particle breakage in ball milling transitions from impact-dominated fracture to attrition-dominated fragmentation. Under high normal impact forces, coarse particles experience induced internal tensile stresses, leading to rapid crack propagation and bulk fracture. Conversely, fine particles resist volume fracture due to reduced flaw density; instead, repeated tangential contacts induce shear stresses along the surface, resulting in progressive material removal through attrition. This transition from impact-controlled fracture to shear-controlled attrition is consistent with the DEM-derived distribution of normal and tangential contact forces.

4.3. Zero-Order Production Characteristic Parameter α

The generation rate of fine particles was plotted on the vertical axis against particle size on the horizontal axis in a double-logarithmic coordinate system. Linear regression was performed for the data points under each filling ratio condition, and the slope of the resulting line was defined as the zero-order production characteristic parameter α. This parameter reflects the sensitivity of fine particle generation rates to particle size across different fractions. The results are presented in Figure 13. The corresponding statistical parameters of the zero-order production characteristic function are summarized in Table 8.

Before conducting the linear regression of the fine particle generation rate against particle size to calculate the zero-order production characteristic parameter α, it is necessary to first obtain the fine particle generation rate through a preliminary linear regression. As a result, experimental and computational errors are compounded, leading to a marginally lower fitting accuracy for α in comparison to the generation rate function. Nevertheless, this does not impact the comparative analysis of α values across varying feed particle sizes.

The mean α values for the finest size fraction during the ceramic ball grinding of coarse, intermediate, and fine magnetite ores were 0.449, 0.596, and 0.614, respectively, indicating notable differences among feed particle sizes, while the filling ratio had no significant effect on α for any fraction. This can be attributed to the dominant breakage mechanisms: normal impact forces for coarse magnetite ore, and tangential grinding forces for intermediate and fine magnetite ores. Therefore, the zero-order production characteristic parameter of the finest size fraction exhibits variation depending on the feed

particle size. These results further confirm that the zero-order production characteristics of fine particles during the ceramic ball grinding of magnetite ore are not wholly independent of the grinding environment.

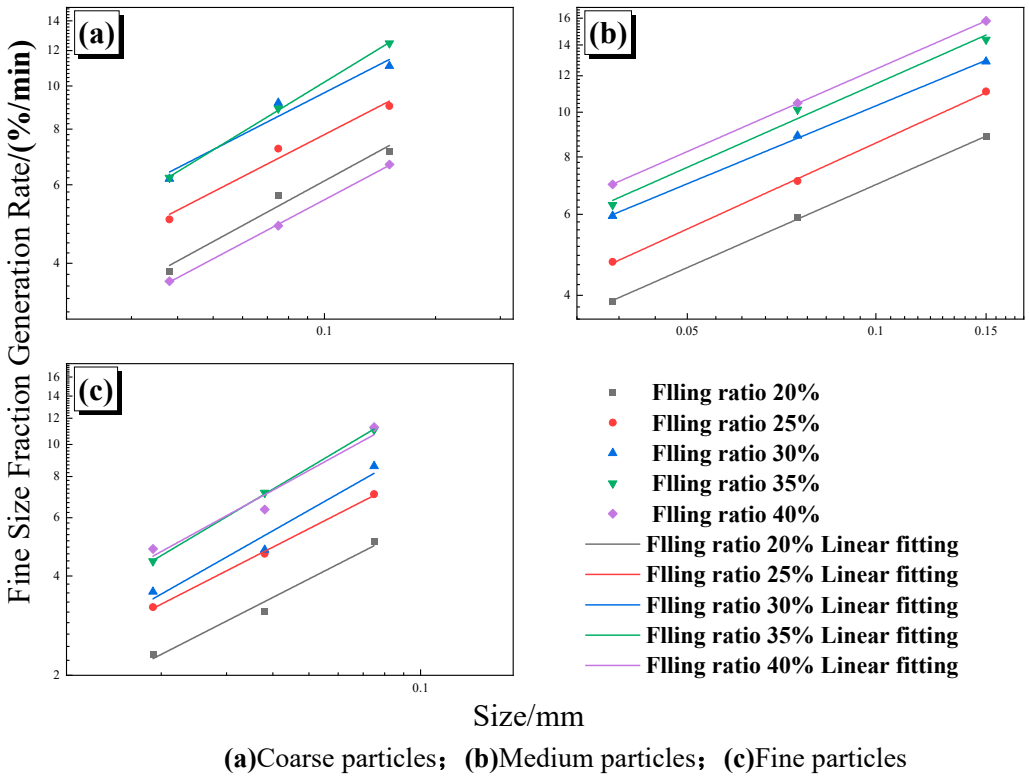


Figure 13. The zero-order production characteristic parameter α under different filling ratios.

Table 8. Statistical parameters of the zero-order output characteristic function for ceramic ball grinding of magnetite ore with different feed size classes.

Filling Ratio/%		20	25	30	35	40
Coarse	Intercept	1.238	1.317	1.408	1.513	1.184
	Slope (α)	0.451	0.426	0.424	0.505	0.439
	R^2	0.976	0.978	0.959	0.999	0.999
	adj.R^2	0.953	0.957	0.919	0.999	0.999
	p-value (α)			0.670		
Intermediate	Intercept	1.441	1.554	1.576	1.664	1.688
	Slope (α)	0.598	0.621	0.562	0.602	0.595
	R^2	1.000	0.999	0.999	0.991	1.000
	adj.R^2	1.000	0.999	0.998	0.982	1.000
	p-value (α)			0.766		
Fine	Intercept	1.338	1.491	1.630	1.798	1.724
	Slope (α)	0.573	0.574	0.637	0.668	0.617
	R^2	0.980	0.999	0.962	1.000	0.958
	adj.R^2	0.961	0.997	0.924	0.999	0.917
	p-value (α)			0.187		

4.4. Energy–Size Model

The ceramic ball filling ratio determines the total mass of grinding media in the mill, which directly affects the mill's energy consumption. Therefore, the filling ratio serves as a crucial factor influencing the energy efficiency of the grinding process. Figure 14 illustrates the energy distribution under varying ceramic ball filling ratios, offering essential data for the subsequent development of an energy–particle size model.

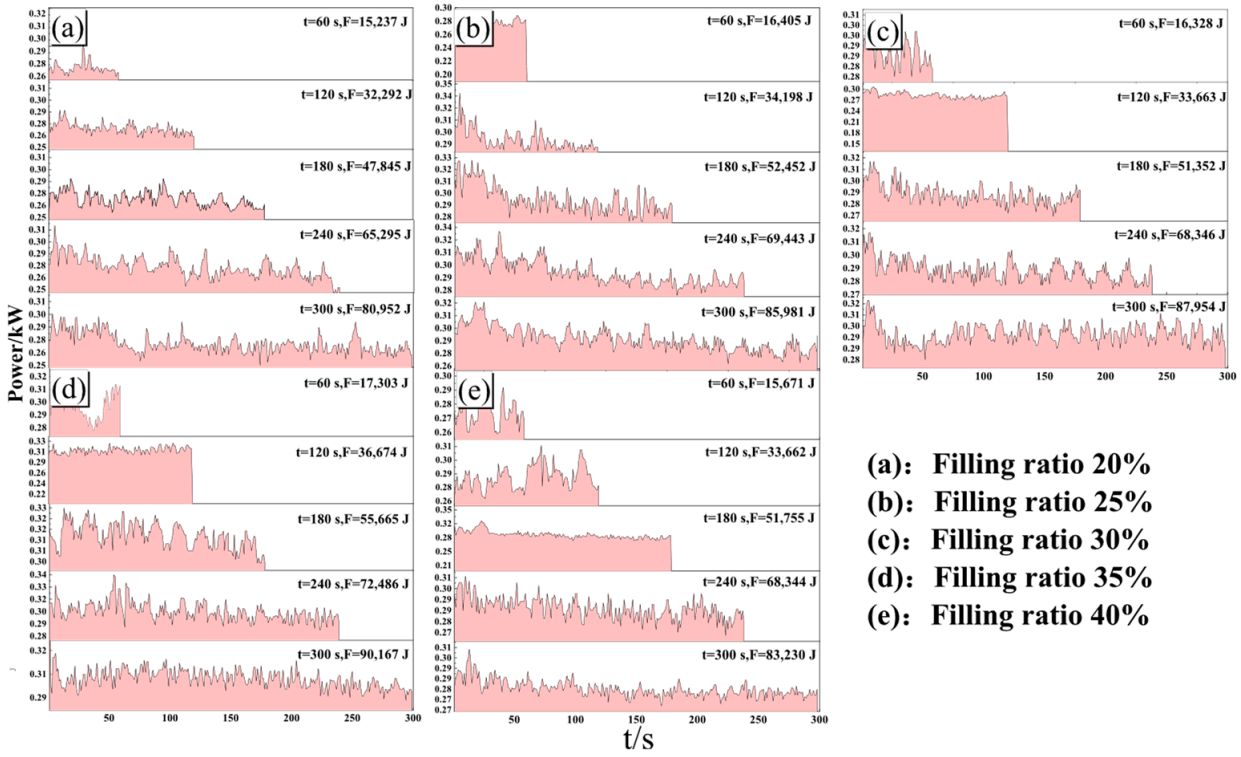


Figure 14. Differences in energy consumption of ceramic ball grinding under different filling ratios.

In a laboratory, multiple large-scale experimental devices operate concurrently, which may result in slight fluctuations in the mill input voltage and minor variations in power. However, when energy consumption experiments under different filling ratios are conducted over a short period, the overall trends remain largely unaffected. Figure 14 presents the energy consumption characteristics of magnetite ore during ceramic ball grinding at different filling ratios:

20% filling ratio: 15,237 J at 60 s, 80,952 J at 300 s, and power 0.26–0.29 kW;

25% filling ratio: 16,405 J at 60 s, 85,981 J at 300 s, and power 0.28–0.33 kW;

30% filling ratio: 16,328 J at 60 s, 87,954 J at 300 s, and power 0.28–0.33 kW, a trend similar to 25%;

35% filling ratio: 17,303 J at 60 s, 90,167 J at 300 s (first time exceeding 90,000 J), and power 0.29–0.34 kW, maximum energy consumption;

40% filling ratio: 15,671 J at 60 s, 83,230 J at 300 s, and power 0.27–0.31 kW, slight decrease in energy consumption.

Figure 15 shows a coordinate system with mill input energy on the vertical axis and grinding time on the horizontal axis, providing a basis for analyzing the energy–particle size relationship.

As illustrated in Figure 15, the total energy input to the mill increases approximately linearly with grinding time. The linear regression analysis between grinding time and input energy demonstrates that the mill's power at a filling ratio of 20% is 0.274 kW. Since the power remains nearly constant over short periods, it can be considered independent of time and thus serves as a valid substitute for the generation rate of the finest size fraction. Based on this approach, the fine particle generation rate function can be reformulated as a function of mill input power P, facilitating the development of an energy–particle size model for the ceramic ball grinding of magnetite ore.

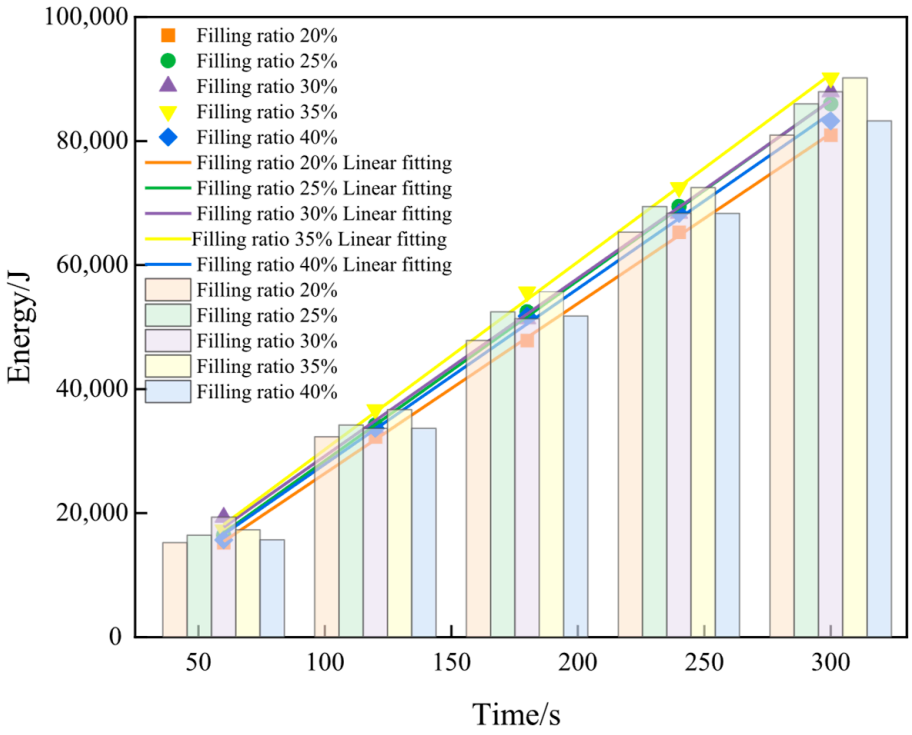


Figure 15. Characteristics of average power for ceramic ball grinding (all linear fittings show excellent agreement with R^2 values ranging from 0.997 to 0.999).

Considering that only approximately 3% of the total input energy is utilized for ore breakage, with the remainder mainly expended on media motion and friction, the influence of particle size on energy consumption can be neglected. With this assumption in mind, the yield of fine particles for varying different feed sizes can be described by a corresponding energy–size model, as follows:

$$m_j(w) = 14.036w + 21.446; -2.360 + 1.180\text{mm} \quad (5)$$

$$m_j(w) = 14.193w + 23.712; -1.180 + 0.600\text{mm} \quad (6)$$

$$m_j(w) = 8.467w + 17.727; -0.600 + 0.300\text{mm} \quad (7)$$

where $m_j(w)$ represents the yield of the finest particle fraction at an input energy w, expressed in %; w denotes the mill input energy in kJ.

Using this approach, energy–size models for different filling ratios can be established, and the corresponding results are presented in Table 9.

Table 9. Energy–size models for different filling ratios.

Ball Filling/%		20%	25%	30%	35%	40%
$m_j(w)$	Coarse	$14.036w + 21.446$	$17.31w + 18.297$	$21.486w - 4.631$	$20.616w + 8.427$	$12.926w + 10.829$
	Intermediate	$14.193w + 23.712$	$16.31w + 19.93$	$20.677w - 1.887$	$20.825w + 10.268$	$24.723w + 19.589$
	Fine	$8.467w + 17.727$	$11.09w + 16$	$12.441w + 3.529$	$14.627w + 9.37$	$17.124w + 16.295$

5. Conclusions

This study examines the characteristics of fine particle production of magnetite during ceramic ball grinding and systematically investigates the influence of the media filling ratio on fine particle generation behavior. The principal conclusions are as follows:

1 Under varying feed size conditions, the media filling ratio has a limited impact on the zero-order production characteristics of fine particles during the ceramic ball grinding of magnetite. For coarse and intermediate feed sizes, the cumulative yield of the finest size fraction demonstrates a robust linear correlation with grinding time, with adjusted R^2 values consistently exceeding 0.99. Within the filling ratio range of 20%–40%, and regardless of the occurrence of repeated breakage, the zero-order production behavior of fine particles remains stable. This indicates that fine particle fractions in ceramic ball grinding products generally exhibit distinct zero-order production characteristics across different filling ratios.

2 The media filling ratio has a significant role in regulating the generation rate of the finest size fraction. An appropriate increase in the filling ratio enhances the generation of fine particles, whereas excessively high filling ratios can inhibit the production of the finest fraction when processing coarse magnetite feeds. For coarse feed sizes, the generation rate of the finest fraction reaches a maximum value of 6.23%/min at a filling ratio of 35% and decreases to 3.65%/min when the filling ratio increases to 40%. When the feed size is smaller than 1.18 mm, the generation rate of the finest fraction shows a pronounced positive correlation with the ceramic ball filling ratio. As the filling ratio increases from 20% to 40%, the generation rate rises from 3.89%/min to 6.97%/min for the −1.18 + 0.60 mm feed size and from 2.32%/min to 4.83%/min for the −0.60 + 0.30 mm feed size.

3 Based on the functional relationship between the generation rate of the finest size fraction and the mill input power, an energy–particle size model for the grinding of magnetite ceramic balls has been established. This model quantitatively describes the variation in the yield of the finest size fraction in relation to both input energy and media filling ratio. The proposed model facilitates effective predictions of the yield of the finest particles under varying filling ratios, providing a robust theoretical foundation for optimizing the media filling ratio, enhancing fine grinding performance, and controlling overgrinding in industrial applications. Such optimization can improve energy utilization efficiency in grinding circuits, contributing to more sustainable mineral processing practices and aligning with the long-term objective of reducing carbon intensity in the mineral industry.

Author Contributions: Methodology, C.Y.; software, Q.L.; formal analysis, C.Y.; investigation, L.S. and Z.Z. (Ziyu Zhou); resources, C.W.; data curation, L.L.; writing—original draft preparation, L.L.; writing—review and editing, C.W. and Z.Z. (Zongyan Zhou); visualization, L.L.; supervision, C.Y.; project administration, C.W.; funding acquisition, C.Y. All authors have read and agreed to the published version of the manuscript.

Funding: This research was funded by National Natural Science Foundation of China (grant number No. 52504293), and Research Startup Project of Jiangxi University of Science and Technology (grant number No. jxust-45). The APC was funded by National Natural Science Foundation of China.

Data Availability Statement: Data is available on request.

Acknowledgments: We appreciate the constructive comments provided by the anonymous reviewers and editors of this journal, which significantly improved the quality of the manuscript.

Conflicts of Interest: The authors declare no conflict of interest.

References

1. Austin, L.G.; Klimpel, R.R.; Luckie, P.T. *Process Engineering of Size Reduction: Ball Milling*; SME: Denver, CO, USA, 1984.
2. Wills, B.A.; Napier-Munn, T.J. *Mineral Processing Technology*; Elsevier: Amsterdam, The Netherlands, 2015.
3. Tang, Y.H.; Dong, W.M.; Jin, Y. The Experimental Analysis of Rotation Speed and Medium Filling Rate on Grinding Performance to a Horizontal Stirred Mill. *Appl. Mech. Mater.* **2015**, *779*, 80–83. [CrossRef]

4. Guo, W.; Han, Y.; Li, Y.; Tang, Z. Impact of ball filling rate and stirrer tip speed on milling iron ore by wet stirred mill: Analysis and prediction of the particle size distribution. *Powder Technol.* **2021**, *378*, 12–18. [CrossRef]
5. Bond, F.C. *Crushing and Grinding Calculations; Additions and Revisions*; Allis-Chalmers Manufacturing Co.: Milwaukee, WI, USA, 1962.
6. Kesall, D.F. Continuous Grinding in a Small Wet Ball Mill Part II. A Study of the Influence of Hold-Up Weight. *Powder Technol.* **1968**, *69*, 162–168.
7. Tang, B.L.; Cheng, B.; Song, X.Z.; Ji, H.A.; Li, Y.J.; Wang, Z.H. Experimental Study on the Influence of Rotational Speed on Grinding Efficiency for the Vertical Stirred Mill. *Minerals* **2024**, *14*, 1208. [CrossRef]
8. Cleary, P.W. Recent advances in dem modelling of tumbling mills. *Miner. Eng.* **2001**, *14*, 1295–1319. [CrossRef]
9. Gupta, V.K. Population balance modeling approach to determining the mill diameter scale-up factor: Consideration of size distributions of the ball and particulate contents of the mill. *Powder Technol.* **2022**, *395*, 412–423. [CrossRef]
10. Yu, P.; Xie, W.; Liu, L.X.; Hilden, M.; Powell, M.S. A consolidated summary on the evolution of a dynamic tumbling mill model. *Powder Technol.* **2021**, *391*, 173–183. [CrossRef]
11. Bwalya, M.M.; Samukute, O.S.; Chimwani, N. SAG Mill Grinding Media Stress Evaluation-A DEM Approach. *Minerals* **2025**, *15*, 431. [CrossRef]
12. Li, Y.; Xiao, Q.; Wang, G.; Sun, B.; Zheng, C.; Jin, S.; Wang, Q. SAG mill ball diameter semi-theory based on pebble fracture strength and DEM validation. *Miner. Eng.* **2025**, *222*, 109169. [CrossRef]
13. Wang, G.B.; Xiao, Q.F.; Wang, X.J.; Li, Y.X.; Jin, S.Z.; Wang, M.T.; Shao, Y.F.; Zhang, Q.; Pei, Y.J.; Liu, R.T. Research on Optimization of Lifter of an SAG Mill Based on DEM Simulation and Orthogonal Tests and Applications. *Minerals* **2025**, *15*, 193. [CrossRef]
14. Rajodiya, P.; Harichandan, B.; Dave, S.; Sharma, K.; Banerjee, G.; Chattopadhyay, S. Investigating the impact of grinding media shape on load behaviour and mill power in an industrial-scale tumbling mill using DEM simulation. *Miner. Eng.* **2025**, *234*, 109717. [CrossRef]
15. Tong, J.Q.; Wu, C.B.; Wang, Y.H.; Tian, J.K.; Li, Z.Y.; Xie, F.; Yao, X.; Zeng, G.S. Effect on Fine Particles Output Characteristics of Ceramic Ball Grinding. *Minerals* **2023**, *13*, 1416. [CrossRef]
16. Zhang, X.; Wei, H.; Han, Y.; Zhou, Z.; Li, W. Effect of different mills on the fine grinding characteristics and leaching behaviour of gold ore. *Miner. Eng.* **2024**, *215*, 108800. [CrossRef]
17. Zhang, H.; Li, Y. Effects of Grinding Parameters on Particle Size Distribution and Fine Generation. *Minerals* **2024**, *14*, 618. [CrossRef]
18. Yuan, C.; Wu, C.; Ling, L.; Yao, X.; Li, Z.; Xie, F.; Tian, J. Ceramic Grinding Kinetics of Fine Magnetite Ores in the Batch Ball Mill. *Minerals* **2023**, *13*, 1188. [CrossRef]
19. Panayotova, M. Control of Non-Ferrous Metal-Sulfide Minerals' Flotation via Pulp Potential. *Minerals* **2023**, *13*, 1512. [CrossRef]
20. Guo, M.C.; Yang, Y.K.; Yu, S.L.; Wu, Y.M.; Gu, G.H.; Wang, Y.H.; Li, Q.K.; Chen, J.Y. Effects of Grinding Parameters on Galena Particle Size Distribution and Flotation Performance. *Minerals* **2025**, *15*, 618. [CrossRef]
21. Tong, J.; Wu, C.; Yuan, C.; Cheng, Y.; Xing, Y.; Zeng, G.; Zhou, Z.; Geng, Z. Microscopic Mechanisms and Surface Properties Behind the Enhanced Flotation of Pyrite Using Ceramic and Steel Balls. *Colloids Surf. A Physicochem. Eng. Asp.* **2025**, *713*, 136494. [CrossRef]
22. Li, Q.K.; Wu, Y.M.; Lv, B.C.; Ouyang, C.Z.; Wu, L.D.; Wang, Y.H.; Gu, G.H.; Yang, Y.K. Fine-grinding media control chalcocite flotation through surface electrochemistry. *Miner. Eng.* **2026**, *236*, 109960. [CrossRef]
23. Samenova, N.; Daulet, B.; Tussupbayev, N.; Turysbekov, D.; Narbekova, S. Influence of emulsion microbubbles on the flotation recovery of fine-dispersed chalcopyrite. *Miner. Eng.* **2026**, *237*, 110052. [CrossRef]
24. Nilssen, B.E.; Kleiv, R.A.; Henriksen, B.R. The distribution of oxygen in submicron silicon powders produced by ultrafine grinding. *Powder Technol.* **2023**, *427*, 118657. [CrossRef]
25. Yan, W.P.; Zhang, B.Y.; Yang, Y.H.; Deng, J.; Li, W.S. The Cavitation Characteristics of Micro-Nanobubbles and Their Effects on the Flotation Recovery of Fine-Grained Ilmenite. *Minerals* **2025**, *15*, 628. [CrossRef]
26. Zhang, X.; Qin, Y.; Jin, J.; Li, Y.; Gao, P. High-efficiency and energy-conservation grinding technology using a special ceramic-medium stirred mill: A pilot-scale study. *Powder Technol.* **2022**, *396*, 354–365. [CrossRef]
27. Yuan, C.; Wu, C.; Fang, X.; Liao, N.; Tong, J.; Yu, C. Effect of Slurry Concentration on the Ceramic Ball Grinding Characteristics of Magnetite. *Minerals* **2022**, *12*, 1569. [CrossRef]
28. Fang, X.; Wu, C.; Liao, N.; Yuan, C.; Zhong, J.; Zhu, S.; Liu, A.; Xiao, K. Understanding the Energy-Saving mechanism of ceramic balls in tumbling mills. *Miner. Eng.* **2024**, *218*, 108982. [CrossRef]
29. Fang, X.; Wu, C.; Liao, N.; Ling, L.; Wu, J.; Liu, R.; Lu, D.; Wang, H.; Li, B. Research on mixed steel and ceramic balls in tumbling mills: Motion behavior and energy evolution. *Powder Technol.* **2025**, *452*, 120576. [CrossRef]
30. Fang, X.; Wu, C.; Yuan, C.; Liao, N.; Chen, Z.; Li, Y.; Lai, J.; Zhang, Z. Can ceramic balls and steel balls be combined in an industrial tumbling mill? *Powder Technol.* **2022**, *412*, 118020. [CrossRef]

31. Yu, J.; Sun, H.; An, Y.; Gao, P.; Zhang, X.; Han, Y. Energy conservation and consumption reduction in grinding operations through ceramic media stirring mill: An industrial validation test. *Powder Technol.* **2023**, *429*, 118943. [CrossRef]
32. Medina-Pierres, J.; Menéndez-Aguado, J.M.; Fulla, M.R.; Rivera, I.E. Generalized mathematical model applied to a silica sand laboratory-controlled mill: Derivation of simplified ceramic ball entrance flux, ball wear consumption, and mass distribution functions. *Miner. Eng.* **2024**, *219*, 109055. [CrossRef]
33. Wu, C.; Chen, Z.; Liao, N.; Tian, J.; Xie, F.; Zeng, G. Enhancing the Grinding Efficiency of a Magnetite Second-Stage Mill through Ceramic Ball Optimization: From Laboratory to Industrial Applications. *Minerals* **2024**, *14*, 160. [CrossRef]
34. Zhao, Q.F.; Zhang, Y.H.; Gao, P.; Tong, L.L.; Han, Y.X.; Yang, H.Y.; Yuan, S. Mitigating iron contamination in cyanide gold extraction: Ceramic grinding media for enhanced efficiency and reduced cyanide consumption. *Miner. Eng.* **2025**, *234*, 109779. [CrossRef]
35. Fan, L.; Tong, X.; Xie, X.; Liu, D.; Yao, R. Experimental Study on Combined Magnetic-Gravity Separation of a Low-grade Ilmenite Ore in Yunnan. *Nonferrous Met. (Miner. Process. Sect.)* **2025**, *11*, 41–49.
36. Chen, F.; Shi, S.; Fan, X.; Sun, W. Experimental Study on Enhancing Ilmenite Recovery with Fine Particle Flotation Equipment. *Nonferrous Met. (Miner. Process. Sect.)* **2025**, *10*, 127–134.
37. Jia, W.; Zhou, Y.; Lu, Y.; Chen, W. Progress in Processing Technologies for Ultrafine Iron Ores. *Nonferrous Met. (Miner. Process. Sect.)* **2025**, *9*, 55–66.
38. Durgut, E. Industrial-Based Comprehension on the Ceramic Body Composition by Continuous/Batch Grinding Methods. *Minerals* **2025**, *15*, 1070. [CrossRef]
39. Liu, S.C.; Lu, J.F.; Xu, H.Y.; Yuan, C.F.; Xu, J.; Dianyu, E.; Liu, S.D.; Zhou, Z.Y. Performance analysis of mixtures of ceramic and steel grinding balls in an industrial scale semi-autogenous mill. *Powder Technol.* **2025**, *466*, 121428. [CrossRef]
40. Zhao, R.; Han, Y.; He, M.; Li, Y. Grinding kinetics of quartz and chlorite in wet ball milling. *Powder Technol.* **2017**, *305*, 418–425. [CrossRef]
41. Cavarretta, I.; O'Sullivan, C.; Ibraim, E.; Lings, M.; Hamlin, S.; Wood, D.M. Characterization of artificial spherical particles for DEM validation studies. *Particuology* **2012**, *10*, 209–220. [CrossRef]
42. Laurent, B.F.C.; Cleary, P.W. Comparative study by PEPT and DEM for flow and mixing in a ploughshare mixer. *Powder Technol.* **2012**, *228*, 171–186. [CrossRef]
43. Cundall, P.A.; Strack, O.D. A discrete numerical model for granular assemblies. *Geotechnique* **1979**, *29*, 47–65. [CrossRef]

Disclaimer/Publisher's Note: The statements, opinions and data contained in all publications are solely those of the individual author(s) and contributor(s) and not of MDPI and/or the editor(s). MDPI and/or the editor(s) disclaim responsibility for any injury to people or property resulting from any ideas, methods, instructions or products referred to in the content.